Flamelet structures in spray ignition

By J. Urzay, D. Martínez-Ruiz, A. L. Sánchez, A. Liñán AND F. A. Williams

1. Motivation and objectives

In typical liquid-fueled burners the fuel is injected as a high-velocity liquid jet that breaks up to form the spray. The initial heating and vaporization of the liquid fuel rely on the relatively large temperatures of the surrounding gas, which may include hot combustion products and preheated air. The heat exchange between the liquid and the gas phases is enhanced by droplet dispersion arising from the turbulent motion. Chemical reaction takes place once molecular mixing between the fuel vapor and the oxidizer has occurred in mixing layers separating the spray flow from the hot air stream. Since in most applications the injection velocities are much larger than the premixed-flame propagation velocity, combustion stabilization relies on autoignition of the fuel-oxygen mixture, with the combustion stand-off distance being controlled by the interaction of turbulent transport, droplet heating and vaporization, and gas-phase chemical reactions.

In this study, conditions are identified under which analyses of laminar flamelets can shed light on aspects of turbulent spray ignition. This study extends earlier fundamental work by Liñán & Crespo (1976) on ignition in gaseous mixing layers to ignition of sprays. Studies of laminar mixing layers have been found to be instrumental in developing understanding of turbulent combustion (Peters 2000), including the ignition of turbulent gaseous diffusion flames (Mastorakos 2009). For the spray problem at hand, the configuration selected, shown in Figure 1, involves a coflow mixing layer formed between a stream of hot air moving at velocity U_A and a monodisperse spray moving at velocity $U_S \sim U_A$. The boundary-layer approximation will be used below to describe the resulting slender flow, which exhibits different igniting behaviors depending on the characteristics of the fuel. In this approximation, consideration of the case $U_A = U_S$ enables laminar ignition distances to be related to ignition times of unstrained spray flamelets, thereby providing quantitative information of direct applicability in regions of low scalar dissipation-rate in turbulent reactive flows (see the discussion in pp. 181–186 of Peters (2000)).

This report is organized as follows. Effects of droplet dispersion dynamics on ignition of sprays in turbulent mixing layers are discussed in Section 2. The formulation for ignition in laminar mixing layers is outlined in Sections 3 and 4. The results are presented in Section 5. In Section 6, the mixture-fraction field and associated scalar dissipation rates for spray ignition are discussed. Finally, some brief conclusions are drawn in Section 7.

2. Flamelet physics in spray ignition

Before proceeding with the analysis, it is of interest to discuss in greater detail the relevance of the laminar problem investigated below in the context of spray ignition in turbulent mixing layers. The dynamics of the large vortices in the mixing layer is characterized by the integral time scale

$$t_\ell = \ell/U, \tag{2.1}$$

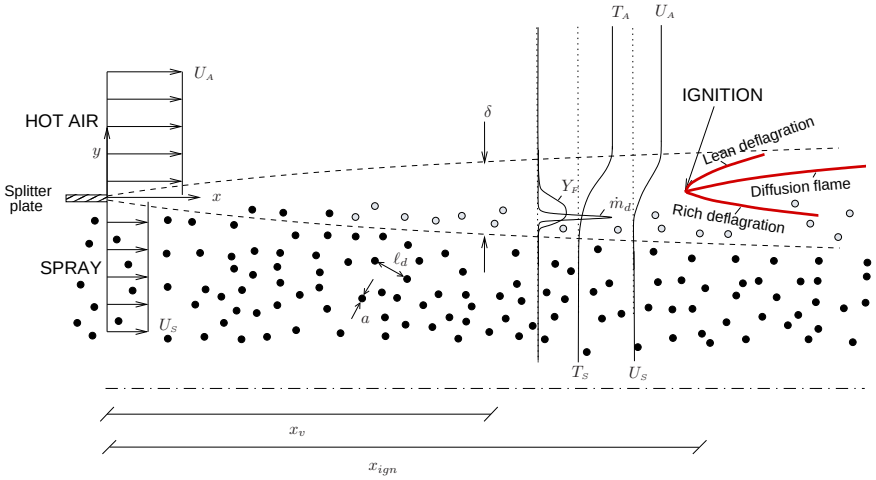

FIGURE 1. Sketch of the model problem: The thermal ignition of a fuel spray in a two-dimensional laminar mixing layer. Here, the black dots indicate fuel droplets, with grey-color droplets corresponding to vaporizing droplets. The dashed lines represent the edges mixing-layer.

with ℓ being the integral length (i.e., the characteristic thickness of the turbulent mixing layer) and U being related to the mean streamwise velocity. This time is to be compared with the characteristic acceleration time of the droplets. When the motion around the droplet is dominated by molecular transport, as occurs when the droplets are sufficiently small, this acceleration time (or Stokes time) is of the order of the droplet vaporization time, defined below in (3.2), which can be therefore used to define an integral-scale Stokes number

$$\mathrm{St} = t_v/t_\ell, \tag{2.2}$$

a parameter controlling the overall dispersion characteristics in particle-laden turbulent mixing layers. Different values of St are associated with different regimes of droplet dispersion, as depicted in Figure 2(a-c).

For $\mathrm{St} \gg 1$ the droplets on the spray side of the mixing layer are insensitive to the velocity perturbations induced by the large vortical motion and therefore continue in straight trajectories, as sketched in Figure 2(b). In this slip regime, which is not of much technological relevance, the droplets remain surrounded by the cold carrier gas, thereby hindering droplet vaporization and spray ignition.

Droplet dispersion becomes optimal for $\mathrm{St} = O(1)$, when the compression strain effect acting in times of order t_ℓ enables the droplets to be ejected from the spray side through the high-strain vortex-braid regions, resulting in non-uniform droplet distributions. Experimental visualizations of these preferential-concentration effects on particle-laden turbulent flows have been reported in earlier work (see, for instance, Longmire & Eaton (1992)). In this scenario, which is depicted in Figure 2(c), the droplets cross the mixing layer to vaporize on the other side surrounded by hot air. Individual-droplet ignition is seldom observed for droplets in the sub-millimeter diameter range, because at the air temperatures typically found in applications the characteristic chemical time for ignition is much larger than the diffusion time around the droplet. Instead, the fuel vapor generated by droplet vaporization mixes with the surrounding air to form reactive pockets that are convected downstream. If the fuel concentration in these pockets is sufficiently high for the resulting mixture to be flammable, ignition occurs downstream, at a location

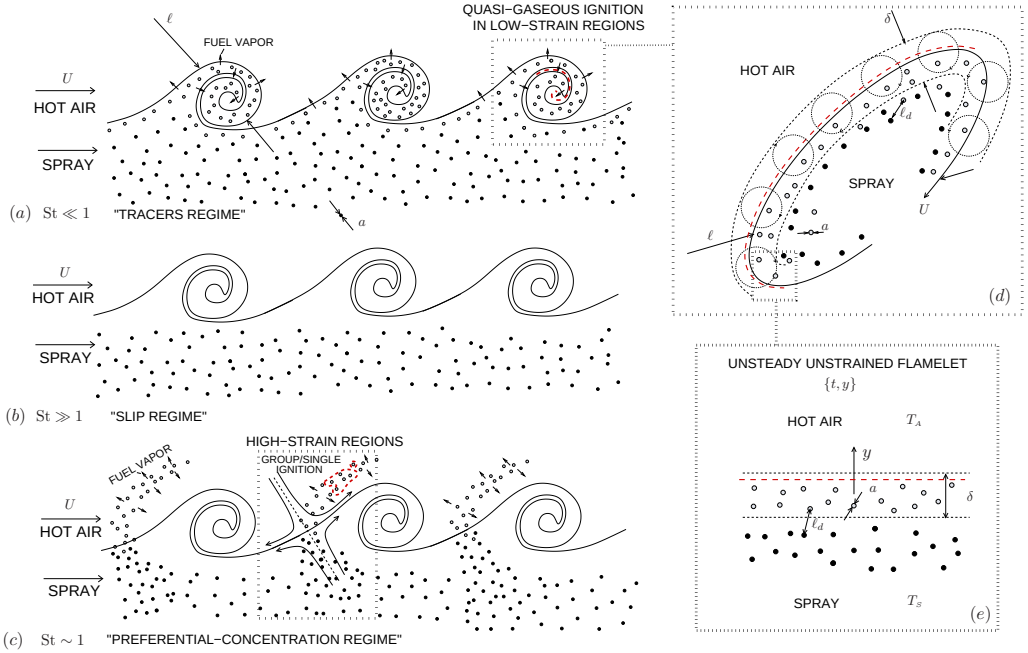

FIGURE 2. Spray ignition in turbulent mixing layers at (a) small Stokes numbers (tracers regime), (b) large Stokes numbers (slip regime) and (c) order-unity Stokes numbers (preferential-concentration regime). Figure (d) shows a sketch of the large turbulent eddies entraining the fuel spray, and (e) depicts the unsteady unstrained flamelet model of spray ignition at low Stokes numbers. Igniting regions are sketched with thick-dashed lines (red color online).

such that the residence time becomes comparable to the chemical time for homogeneous ignition. In this regime, conditions for individual-droplet combustion or droplet-cloud combustion may occur, the latter being favored by large mass-loading ratios.

The description of ignition for $\mathrm{St} = O(1)$ is not readily amenable to a simple Eulerian modeling of the type used here because of the existence of crossing droplet trajectories as the droplets traverse the mixing layer through the vortex braids. These crossing trajectories have been observed, for instance, in counterflow configurations (Li 1997), which resemble -to some extent- the high-strain field of the vortex-braid regions in turbulent mixing layers, and which are often used for premixed and non-premixed flamelet modeling of turbulent gaseous flames (Peters 2000). In spray counterflow configurations at $\mathrm{St} = O(1)$, however, flamelet modeling becomes difficult, because, in addition to the trajectory crossing, the solution is sensitive to the thermal and kinematic conditions of the spray far from the stagnation plane, with the distance of injection being an additional parameter in the formulation.

For $\mathrm{St} \ll 1$, the droplets behave as flow tracers and become entrained in the large-scale turbulent eddies, where they come into contact with the high-temperature air, thereby promoting vaporization and ignition of the fuel spray in the resulting mixing layers. This regime is depicted in Figure 2(a). The strain in the vortex-braid regions promotes the transport of the fuel vapor toward the interior of the rollers, where ignition occurs more readily as a result of the existing lower strain (Wang & Rutland 2007; Mastorakos 2009), whereas the larger strain rates found in the vortex-braid regions prevent ignition from occurring there by limiting fuel residence times. As suggested earlier for purely gaseous

ignition (Peters 2000), the unstrained flamelet, shown in Figure 2(a,b), and achieved in Figure 1 by setting U_S equal to U_A, may provide an adequate representation of the ignition dynamics in the low-strain mixing regions wrapped around the core of such large vortices. As a consequence, associated ignition times, as those computed below, are relevant for quantifying ignition distances in these turbulent mixing layers.

The above discussion revolves around the effect of the large eddies associated with the integral scales of the turbulent mixing layer, which dominate the dispersion of the droplets. These large eddies coexist and interact with smaller eddies, with the smallest size corresponding to the Kolmogorov length scale ℓ_k, which can be anticipated to be comparable to the laminar mixing-layer thickness δ in the model of Figure 1, because both lengths are influenced by molecular-transport effects. Although these smaller turbulent eddies may also affect mixing and reaction, their effect on ignition is less prominent than that of the large vortices, in that the cores of the large rollers correspond to regions of low strain, where ignition should occur sooner and where the unstrained laminar flamelet provides a good representation for the local flow.

Changes to the general two-continua formulation used below would be needed in analyzing turbulent flows when the Kolmogorov length scale ℓ_k attains sufficiently small values. For instance, for values of ℓ_k comparable to or smaller than the interdroplet distance ℓ_d, the following homogenized treatment of the droplet population is no longer a valid approximation, and rather than attempting to generalize it, a more efficient approach may be to introduce a Lagrangian description of individual droplets. For even smaller values of ℓ_k, of the order of the droplet radius a, unsteady effects of turbulent motion in the immediate vicinity of the droplet should be retained to calculate the forces acting on and the heating and vaporization rates of the droplets, thereby complicating significantly the description. The following development therefore precludes ℓ_k from being smaller than δ, analyses with $U_S \neq U_A$ reflecting some of the aspects of influences of strain in Kolmogorov eddies.

3. Characteristic scales

The characteristic mass-loading ratio, i.e., the ratio of the mass of liquid per unit volume to the gas density, can be evaluated from

$$\alpha = \frac{4}{3}\pi a_o^3 n_o \rho_l / \rho_A, \tag{3.1}$$

for this configuration, in terms of the liquid-fuel density, ρ_l, the air density in the hot coflow stream, ρ_A, the initial values of the droplet radius, a_o, and of the number of droplets per unit volume in the spray stream, n_o. In combustion applications involving liquid-fuel injection, appreciable liquid heating and vaporization resulting from heat transfer from the gas carrier occurs only downstream from the atomization region, once the droplet distribution becomes sufficiently dilute for the mass-loading ratio to decay to values of order unity. When this condition $\alpha \sim O(1)$ is used in (3.1) the relationship $l_d \sim (\rho_l/\rho_A)^{1/3} a_o \gg a_o$ is obtained for the order of magnitude of the initial inter-droplet distance $l_d = n_o^{-1/3}$, with the ratio of liquid-to-gas densities ρ_l/ρ_A taking up pressure-dependent values as large as $\rho_l/\rho_A \sim 10^3$ for typical subcritical conditions. The largeness of the density ratio ρ_l/ρ_A is central to quasi-steady formulations of vaporization rates in sprays (Liñán 1985). If $\rho_l/\rho_A = O(1)$, as it may occur in supercritical sprays, the vaporization dynamics becomes fully unsteady in droplet scales, a limit which is not considered here.

The scales l_d and $a_o \ll l_d$ are to be compared with those of the spray-air mixing layer, associated with the acceleration, heating and vaporization of the droplets. These three processes have comparable time scales, of the order of the droplet vaporization time

$$t_v = \left(\frac{\rho_l}{\rho_A}\right) \frac{a_o^2}{3D_{T_A}}, \tag{3.2}$$

at low droplet Reynolds numbers, where D_{T_A} is the air-side value of the gas thermal diffusivity. Since the chemical reaction cannot begin until after the gaseous fuel is generated, the vaporization time t_v naturally defines the scales of the igniting mixing layer, in that ignition occurs at distances downstream from the splitter plate that are of the order of or larger than $x_v = U_A t_v$. At these streamwise distances, the characteristic thickness of the mixing layer is $\delta \sim (D_{T_A} t_v)^{1/2} \sim (\rho_l/\rho_A)^{1/2} a_o$, which is smaller than x_v by a factor equal to the square root of the characteristic Péclet number $\mathrm{Pe} = (x_v/\delta)^2 = U_A^2 t_v / D_{T,A}$ For the large values of Pe typically found in applications, the resulting flow is slender and correspondingly can be described in the boundary-layer approximation.

For simplicity, the chemistry describing the ignition process will be modeled with an irreversible reaction between the oxygen of the air and the fuel vapor to produce combustion products according to $\mathrm{F} + s\mathrm{O}_2 \rightarrow (1+s)\mathrm{P} + Q$, where s and Q are, respectively, the mass of oxygen consumed and the amount of heat released per unit mass of fuel burned. A characteristic chemical time for fuel oxidation can be evaluated as

$$t_c = B^{-1} \exp[E_a/(\mathrm{R}^0 T_A)], \tag{3.3}$$

with B a frequency factor, E_a an overall activation energy, and R^0 the universal gas constant. The ratio of this chemical time to the vaporization time defined in (3.2) gives the Damköhler number

$$\Delta = t_v/t_c, \tag{3.4}$$

which enters as an important parameter in the problem.

4. Conservation equations

The vaporization time given in (3.2) is used to define length scales for the longitudinal and transverse coordinates, x and y, giving the dimensionless variables $x' = x/(U_A t_v)$ and $y' = y/(D_{T_A} t_v)^{1/2}$. Correspondingly, the velocity of the gas and that of the droplets are scaled to give $u' = u/U_A$ and $u'_d = u_d/U_A$ for the longitudinal components and $v' = v/(D_{T_A}/t_v)^{1/2}$ and $v'_d = v_d/(D_{T_A}/t_v)^{1/2}$ for the transverse components. The characteristic properties of the air stream are used to scale the gas and droplet temperatures, $T' = T/T_A$ and $T'_d = T_d/T_A$, as well as the gas density, viscosity and thermal conductivity, $\rho' = \rho/\rho_A$, $\mu' = \mu/\mu_A$, and $\kappa' = \kappa/\kappa_A$, respectively. A Fickian description is adopted for the diffusion velocities of all species, with the binary diffusivity of species i into the mixture D'_i scaled with its air-side value to give $D'_i = D_i/D_{iA}$. The primes used above to denote non-dimensional variables are dropped in what follows. A presumed power-law dependence $\rho D_i = \mu = \kappa = T^\sigma$ is introduced for the transport properties, with $\sigma = 0.7$. It is assumed that the molecular mass of the inert gas in the spray stream is close to that of air, so that prior to ignition changes in mean molecular weight of the gas mixture are associated only with the presence of fuel vapor. As a result, the equation of state can be written in terms of the mass fraction of fuel Y_F in the form $\rho T[1 - Y_\mathrm{F}(1 - W_A/W_F)] = 1$, with W_A and W_F representing, respectively, the molecular mass of the air and the fuel.

In terms of the above dimensionless variables, the gas-phase conservation equations

reduce to

$$\frac{\partial(\rho u)}{\partial x}+\frac{\partial(\rho v)}{\partial y}=\alpha n\dot{m}_d, \tag{4.1}$$

$$\frac{\partial(\rho uu)}{\partial x}+\frac{\partial(\rho vu)}{\partial y}=\mathrm{Pr}\frac{\partial}{\partial y}\left(T^\sigma\frac{\partial u}{\partial y}\right)+\alpha n\dot{m}_d u_d-\alpha n f_x, \tag{4.2}$$

$$\frac{\partial(\rho uY_{\mathrm{F}})}{\partial x}+\frac{\partial(\rho vY_{\mathrm{F}})}{\partial y}=\frac{1}{\mathrm{Le}_{\mathrm{F}}}\frac{\partial}{\partial y}\left(T^\sigma\frac{\partial Y_{\mathrm{F}}}{\partial y}\right)+\alpha n\dot{m}_d-\Delta\Omega, \tag{4.3}$$

$$\frac{\partial(\rho u\hat{Y}_{\mathrm{O}})}{\partial x}+\frac{\partial(\rho v\hat{Y}_{\mathrm{O}})}{\partial y}=\frac{\partial}{\partial y}\left(T^\sigma\frac{\partial\hat{Y}_{\mathrm{O}}}{\partial y}\right)-S\Delta\Omega, \tag{4.4}$$

$$\frac{\partial(\rho uT)}{\partial x}+\frac{\partial(\rho vT)}{\partial y}=\frac{\partial}{\partial y}\left(T^\sigma\frac{\partial T}{\partial y}\right)-\alpha n[\dot{m}_d(l_v-T_d)+\dot{q}_d]+q\Delta\Omega, \tag{4.5}$$

where Pr represents the Prandtl number, $S=s/Y_{\mathrm{O}_{2A}}$ is the mass of air consumed per unit mass of fuel burned, $\hat{Y}_O=Y_O/Y_{\mathrm{O}_{2A}}$ is the normalized mass fraction of oxygen, and $q=Q/(c_pT_A)$ and $l_v=L_v/(c_pT_A)$ are the dimensionless values of the heat of combustion (lower heating value) and latent heat of vaporization, respectively, of the fuel. Although a unity Lewis number is assumed for oxygen in writing (4.4), an excellent approximation under most combustion conditions, the formulation considers a fuel-vapor Lewis number Le_{F} different in general from unity, as is necessary to account for the low diffusivity of most spray fuels. The dimensionless chemical reaction rate in (4.3)–(4.5) is given by $\Omega=\rho\hat{Y}_{\mathrm{O}}Y_{\mathrm{F}}\exp[\beta(T-1)/T]$ with $\beta=E_a/(\mathrm{R}^0T_A)$ denoting the nondimensional activation energy.

The accompanying equations for the liquid phase are

$$\frac{\partial(nu_d)}{\partial x}+\frac{\partial(nv_d)}{\partial y}=0,\quad u_d\frac{\partial a^3}{\partial x}+v_d\frac{\partial a^3}{\partial y}=-\dot{m}_d, \tag{4.6}$$

$$a^3\left(u_d\frac{\partial u_d}{\partial x}+v_d\frac{\partial u_d}{\partial y}\right)=f_x,\quad a^3\left(u_d\frac{\partial v_d}{\partial x}+v_d\frac{\partial v_d}{\partial y}\right)=f_y, \tag{4.7}$$

$$ca^3\left(u_d\frac{\partial T_d}{\partial x}+v_d\frac{\partial T_d}{\partial y}\right)=\dot{q}_d, \tag{4.8}$$

where n is the dimensionless droplet-number density, and $c=c_l/c_p$ is the ratio of the specific heats for the two phases. These equations may be derived from the spray equation and associated conservation equations (Williams 1985), for example, by integrating over the droplet size-distribution function, which becomes a delta function for monodisperse sprays.

The values of f_x, f_y, $\dot{q}_d$, and $\dot{m}_d$ are obtained by considering the quasi-steady response of the droplet to the surrounding gaseous atmosphere, whose properties are given by the local values of the gas-phase variables at the droplet location. Specifically, the familiar Stokes law $f_x=(3/2)\mathrm{Pr}T^\sigma a(u-u_d)$ and $f_y=(3/2)\mathrm{Pr}T^\sigma a(v-v_d)$ are used for the force of the gas on the individual droplet on the basis of small droplet Reynolds numbers. Similarly, the associated heating rate and the mass rate of vaporization follow from the analysis of the spherically symmetrical temperature field. The analysis simplifies for fuels whose latent heat of vaporization is much larger than the fuel thermal energy according to $\beta_v=L_vW_F/(\mathrm{R}^0T_B)\gg 1$, as occurs for instance for heptane ($\beta_v=11.02$) and methanol ($\beta_v=12.30$), because, according to the Clausius-Clapeyron relation, the mass fraction of fuel vapor at the droplet surface remains exponentially small until the

droplet temperature reaches values very close to T_B. If the droplets are injected at a temperature $T_S < T_B$, there necessarily exists an initial heat-up period during which all of the heat transferred from the gas phase is employed to increase the droplet temperature from T_S to T_B, without significant vaporization, followed by a vaporization period during which the droplet temperature remains at a value close to the boiling value. According to this simplified two-stage description, which is valid along the droplet lifetime except for a short time interval of order $t_v/\beta_v \ll t_v$ during which simultaneous droplet heating and vaporization occur, the droplet heating and vaporization rates are to be computed according to Liñán (1985) as $\dot{q}_d = aT^\sigma(T - T_d)$ and $\dot{m}_d = 0$ if $T_d < T_B$, and $\dot{q}_d = 0$ and $\dot{m}_d = aT^\sigma \ln[1 + (T - T_B)/l_v]$ if $T_d = T_B$. Here, T_B represents the boiling temperature nondimensionalized with T_A.

Equations (4.1)–(4.5) must be integrated with initial conditions at $x = 0$

$$u - 1 = Y_{\mathrm{F}} = \hat{Y}_{\mathrm{O}} - 1 = T - 1 = n = 0 \tag{4.9}$$

for $y > 0$, and

$$\begin{aligned} u - u_S = Y_{\mathrm{F}} = T - T_S = n - 1 = T_d - T_S = a - 1 \\ = u_d - u_S = v_d = \hat{Y}_{\mathrm{O}} - \hat{Y}_{\mathrm{O}_S} = 0 \end{aligned} \tag{4.10}$$

for $y < 0$, and with boundary conditions for $x > 0$ given by

$$u - 1 = Y_{\mathrm{F}} = \hat{Y}_{\mathrm{O}} - 1 = T - 1 = 0 \tag{4.11}$$

as $y \to +\infty$, and

$$u - u_S = Y_{\mathrm{F}} = \hat{Y}_{\mathrm{O}} - \hat{Y}_{\mathrm{O}_S} = T - T_S = v = 0 \tag{4.12}$$

as $y \to -\infty$, where $\hat{Y}_{\mathrm{O}_S} = 0$ when the spray is carried by an inert gas, and $\hat{Y}_{\mathrm{O}_S} = 1$ when the spray is carried by air.

For the mixing layer, the only relevant flow time is the local residence time, so that the associated Stokes number becomes $\mathrm{St} = 2/(3\mathrm{Pr}\,x)$ in terms of the dimensionless streamwise distance. This decaying function is such that at distances from the splitter plate of order x_v, i.e., dimensionless values $x \sim O(1)$, where ignition is anticipated to occur when $\Delta \gtrsim O(1)$, the resulting Stokes number is of order unity, so that in this region the gaseous streamlines generally differ from the droplet trajectories. For small values of the Damköhler number, however, ignition occurs at distances much larger than x_v, where the local Stokes number is very small, causing the droplet trajectories to follow closely the streamlines up to the ignition point.

5. Fundamental ignition kernels in spray-laden laminar mixing layers

The reactive spray in the laminar mixing layer was computed by numerical integration of (4.1)–(4.5) and (4.6)–(4.8) with the initial and boundary conditions given in (4.9)–(4.12). A Crank-Nicholson numerical scheme was used to integrate the parabolic gas-phase equations by marching in the x direction. The liquid-phase equations were integrated by using a third-order Runge-Kutta method.

The solution depends on the thermochemical and transport properties of the fuel through the values of q, l_v, T_B, c, S, W_A/W_F, and Le_{F}, which are listed in Table 1, where the first four values are evaluated assuming $T_A = 1000$ K for the air-side temperature. The remaining parameters are kept fixed at representative practical values for the simulations unless mentioned otherwise, with values given by $\alpha = 1$, $\mathrm{Pr} = 0.7$, $\Delta = 1$, $\beta = 10$, and

	q	l_v	T_B	c	W_A/W_F	$\mathrm{Le_F}$	S
Heptane	39.5	0.34	0.37	2.2	0.29	2.6	15.2
Methanol	18.6	1.09	0.34	2.5	0.91	1.2	6.5

TABLE 1. Values of the dimensionless parameters used for the two liquid fuels considered.

$T_S = T_B$, the latter implying that the droplets in the spray are in equilibrium with the carrier gas, where no fuel vapor is present. The integrations considered cases with $\hat{Y}_{\mathrm{O}_S} = 0$ and with $\hat{Y}_{\mathrm{O}_S} = 1$, corresponding, respectively, to sprays carried by an inert gas and by air. The discussion below is based on computations for a spray with velocity $u_S = 0.8$. In a recent publication (Martínez-Ruiz *et al.* 2013), additional consideration is given to the isovelocity, unstrained case $u_S = 1.0$, in which a change of reference frame moving with velocity u_S allows formulating the problem in terms of t and y as independent variables. In addition, in that same publication an asymptotic theory of spray ignition is formulated that matches well the numerical results given below.

Sample results of the numerical integrations are shown in Figure 3. In all cases, the spray mixes initially with the coflowing stream of hot air without appreciable chemical reaction. The hot air stream provides the heat needed for droplet vaporization, which, with the scales selected, occurs over distances of order unity. The fuel vapor diffuses into the air stream, and it begins to react with the oxygen as it reaches the high-temperature boundary, located far away from the spray. Different ignition behaviors are observed in Figure 3 depending on the set of parameters selected in the integrations.

5.1. *Non-premixed combustion of sprays carried by inert gas ($\hat{Y}_{\mathrm{O}_S} = 0$)*

Plots of the ignition zone for sprays carried by an inert, shown in Figure 3(a) (heptane) and Figure 3(b) (methanol), display important morphological differences (independent of specific chemical-kinetic properties) depending on the fuel considered, with heptane ignition occurring earlier and in a more abrupt way. Differences in the thermochemical properties of the two fuels explain the different ignition behaviors observed. Thus, because of its smaller latent heat of vaporization ℓ_v, heptane droplets tend to vaporize faster than methanol droplets. As a result, as the mixing layer develops, heptane vapor becomes available for reaction earlier than methanol vapor, thereby explaining the occurrence of ignition at smaller streamwise distances. For example, for the parametric values used in Figure 3(a,b), the resulting ignition distance, identified by the local maximum of the reaction rate, is $x_{ign} \simeq 4.95$ for heptane and $x_{ign} \simeq 14.8$ for methanol.

The ignition of heptane is facilitated by its chemical heat release being more than twice that of methanol, resulting in a larger temperature increase per unit mass of fuel burned that facilitates the self-acceleration of the chemical reaction rate, enabling a thermal runaway to take place. The ignition kernel develops rapidly to produce a diffusion flame surrounded on the sides by lean and rich deflagration waves that burn the excess reactants, a tribrachial structure that is clearly apparent in the reaction-rate contours of Figure 3(a).

The ignition of methanol proceeds in a more gradual form. As a result of the smaller chemical heat release of methanol, when the fuel vapor reaches the hot boundary and reacts with the oxygen of the air, the associated temperature increase is not sufficient to

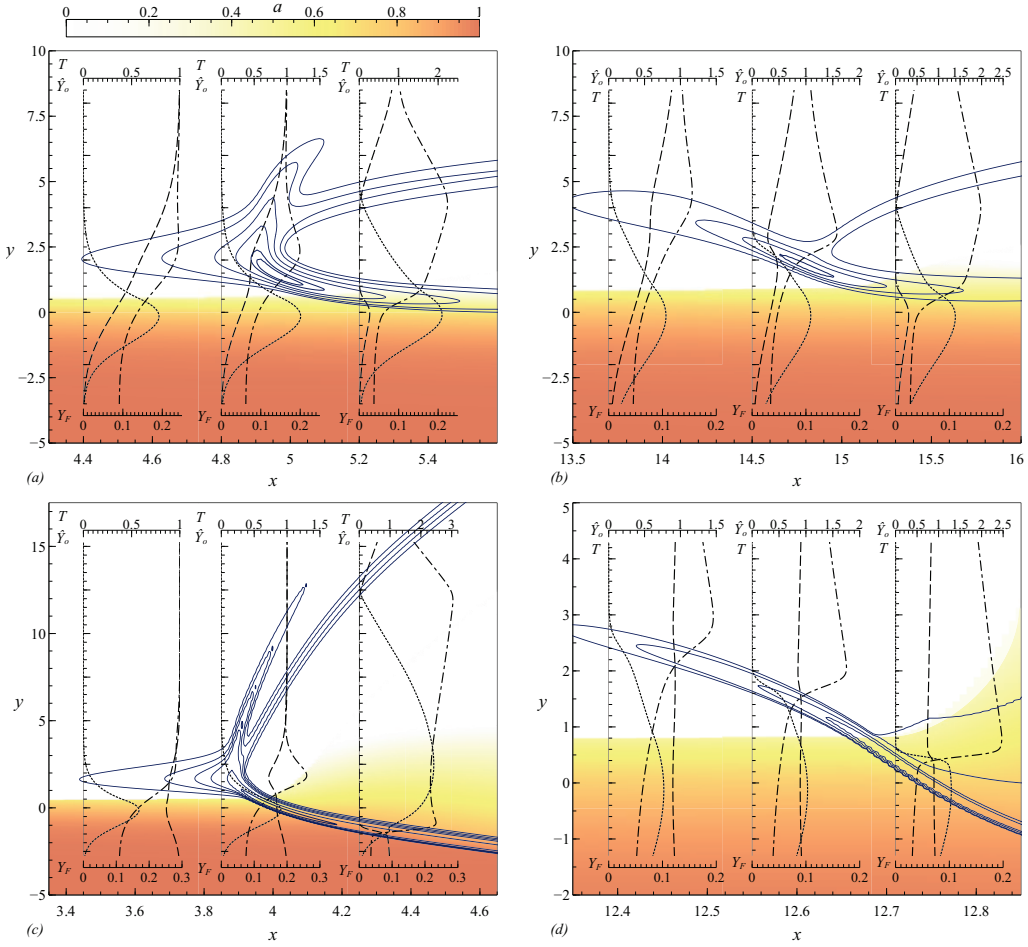

FIGURE 3. Ignition kernels of (a,c) heptane and (b,d) methanol sprays as obtained from integration of (4.1)-(4.7), with q, l_v, T_B, c, S, W_A/W_F, and $\mathrm{Le_F}$ given in Table 1 for each fuel, and $\alpha = 1$, $T_S = T_B$, $u_S = 0.8$, $\mathrm{Pr} = 0.7$, $\Delta = 1$, and $\beta = 10$. The calculations are performed with sprays carried by (a,b) inert gas and (c,d) air. The figures show dimensionless reaction-rate contours (solid lines), with contour lines given by (a) $\Omega = [0.01, 0.02, 0.05, 0.1, 0.2, 0.25]$, (b) $\Omega = [0.02, 0.1, 0.25, 0.5]$, (c) $\Omega = [0.01, 0.025, 0.05, 0.1, 0.5, 2.0]$, and (d) $\Omega = [0.25, 0.5, 2.0, 5.0]$. Shaded contours of the droplet radius a are shown, with dark (red color in online version) and white color indicating $a = 1$ and $a = 0$, respectively. Temperature (dot-dashed lines), fuel mass fraction (dotted lines), and oxygen mass fraction (dashed lines) are shown in the insets for different x locations.

accelerate the chemical reaction locally to produce a thermal runaway. Instead, the fuel is seen to burn in a lean premixed flame that propagates slowly across the mixing layer into richer regions of lower initial temperature. Upon crossing stoichiometric conditions, this slow deflagration wave gives rise to a trailing diffusion flame and to a rich premixed flame, as shown in Figure 3(b). The rich premixed flame increases the rate of spray vaporization as it burns the oxygen pocket that has diffused earlier into the spray side of the mixing layer. This rich flame eventually extinguishes at distances of order unity downstream from the ignition kernel as the oxidizer is depleted.

The two ignition modes identified here, i.e., a thermal runaway and a slow deflagration

propagation, were also encountered in the analysis of ignition in gaseous mixing layers (Liñán & Crespo 1976). In particular, the prevalence of one mode of ignition over the other was found in that case to depend only on the value of the ratio of the temperature difference between the two streams to the temperature increase associated with adiabatic combustion of the stoichiometric mixture, which emerges as the main controlling parameter in the equidiffusional case considered by Liñán & Crespo (1976). A thermal-runaway regime, similar to that found here for heptane, occurs when this ratio takes values smaller than 1. By way of contrast, when its value exceeds unity, the steep temperature gradient found at the ignition kernel prevents the self-acceleration of the chemical reaction from taking place, leading instead to the establishment of a slow lean deflagration, similar to that observed for methanol in Figure 3(b).

5.2. *Partially premixed combustion of sprays carried by air ($\hat{Y}_{\mathrm{O}_S} = 1$)*

Computations of heptane and methanol sprays carried by air were also considered. For heptane, ignition was also seen to occur in this case through a sudden temperature increase, leading to the formation of a triple flame, clearly visible in Figure 3(c). The main difference from Figure 3(a) pertains to the solution that emerges downstream. In Figure 3(a), both premixed branches extinguish at a distance of order unity downstream from the ignition point, as the corresponding deficient reactant is depleted on each side. On the other hand, when air is employed as the spray carrier, the deflagration wave developing on the rich side can propagate continuously into the spray cloud, consuming in a thin reaction layer the oxygen of the air with a fraction of the existing fuel vapor, which is generated on the spray side of the deflagration by heat conduction from the reaction region. The droplets crossing the deflagration vaporize in an oxidizer-free region, producing a large pocket of fuel vapor that has been expanded by the heat release and that diffuses to the air side to burn in a non-premixed flame, and their trajectories now move towards the oxidizer, as can be seen by the expansion of the shaded region. This two-flame structure, resembling that observed in earlier numerical simulations of spray jet flames (Reveillon & Vervisch 2005), is seen to persist downstream from the ignition kernel. The ultimate constant slope of the fuel-rich reaction zone is a measure of the premixed spray deflagration velocity.

A key ingredient for the existence of the two flames depicted in Figure 3(c) is the relatively low value of the heat of vaporization of heptane, which facilitates the generation of a large amount of fuel vapor by droplet vaporization ahead of the deflagration, sufficient to deplete the oxygen of the spray stream, so that an intermediate oxygen-free region appears between the rich deflagration and the diffusion flame. Methanol is less volatile than heptane, and sometimes it does not develop any multiple-flame solution. For instance, in the computation of Figure 3(d), the premixed flame originating near the hot edge of the mixing layer continues burning under lean conditions as it propagates into the spray side, because heat conduction ahead of the front can generate only a limited amount of fuel vapor, as a consequence of the relatively large heat of vaporization of methanol.

5.3. *Interaction of the spray cloud and the deflagration*

The chemical time for the leading deflagration is much smaller than the characteristic chemical time for ignition t_c, defined in (3.3), because the latter is based on the air-side temperature of the mixing layer, which is significantly smaller than the peak flame temperature, as can be seen in the profiles of Figure 3(c,d). As a consequence, with the Damköhler number $\Delta = t_v/t_c$ assumed to be of order unity, the resulting residence time across the flame is smaller than the characteristic vaporization time, so that only

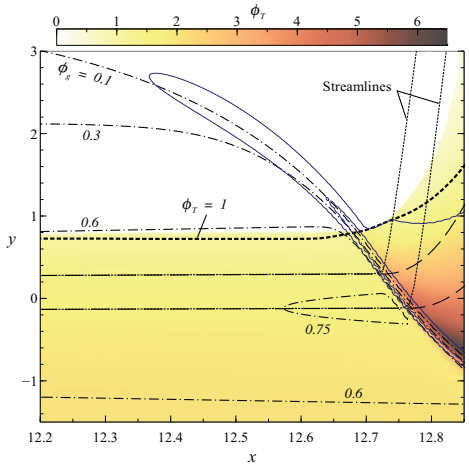

FIGURE 4. Close-up view of the spray-side deflagration wave of Figure 3(d), including droplet trajectories (long-dashed lines), gaseous streamlines (dotted lines), reaction-rate contours $\Omega = 0.1$ and $\Omega = 5$ (solid lines), contours of the gaseous equivalence ratio ϕ_g (dot-dashed lines), and a graded shade to indicate levels of global equivalence ratio ϕ_T (color online).

a relatively small fraction of the liquid fuel vaporizes as the droplets cross the flame. Most of the droplet vaporization occurs instead either upstream in the mixing layer or in the post-flame region, resulting in the distribution of droplet radii shown in the figures. As previously discussed, depending on the value of ℓ_v the associated deflagration can be either rich, as occurs for heptane in Figure 3(c) or lean, as occurs for methanol in Figure 3(d).

A detailed view of the solution near the front corresponding to the flow conditions of Figure 3(d) is given in Figure 4. As the mixing layer develops upstream from the ignition region, the droplets vaporize partially through the heat flux coming from the hot air stream, creating a mixture that, for methanol droplets, is lean everywhere. This is illustrated in Figure 4 by plotting the contours of the gaseous equivalence ratio $\phi_g = SY_F/\hat{Y}_O$. The fuel accumulates toward the middle of the mixing layer, where a maximum value $\phi_g \simeq 0.76$ is achieved. At that intermediate location, the transverse propagation velocity of the deflagration peaks, as indicated by the existence of an inflection point in the curved flame front. Because of the lean conditions, all of the fuel vapor available is consumed across the flame front. The droplets keep vaporizing as they cross the deflagration, and the fuel vapor generated by these droplets burns in a distributed manner in the high-temperature post-flame region with the excess of oxygen that has leaked through the front. The global equivalence ratio $\phi_T = \phi_\ell + \phi_g$, which includes the liquid-based equivalence ratio $\phi_\ell = S\alpha n a^3/(\rho\hat{Y}_O)$, is represented by use of a graded shade in the plot as well as a thick dotted line indicating the region where $\phi_T = 1$.

6. Mixture fractions and scalar dissipation rates in the igniting mixing layer

Mixture fractions and magnitudes of their gradients, called scalar-dissipation rates or, more briefly, scalar dissipation (based on appearance in conservation equations for averages), are widely used in computations, analyses, and modeling of turbulent combustion (Peters 2000). It is important to recognize that there are many different definitions of mixture-fraction fields. They are introduced most readily for two-stream problems, that

is, for problems in which inlet streams are of only two distinct types, typically one containing fuel and the other oxidizer, all fuel streams having identical compositions, and similarly for all oxidizer streams. The most basic definition of a mixture-fraction field is the fraction of mass of the material at any given position and time that originated in one of the two streams (by convention, the fuel stream). In sprays, the mixture fraction may or may not include the liquid fuel (Bilger 2011).

6.1. *The gas-phase mixture fraction in spray combustion*

An alternative definition of a mixture fraction in spray combustion is one that focuses only on the gas phase. This mixture fraction and its corresponding conservation equation can be derived by considering a linear combination of the conservation equations for oxygen and fuel vapor that is free from the chemical source term. The essential results can be illustrated by taking the Lewis number of the fuel to be unity, which simplifies the equations, but is not a necessary assumption (Arrieta-Sanagustín *et al.* 2013; Martínez-Ruiz *et al.* 2013). With this simplification, adding (4.4) and (4.3) times S leads, after use is made of (4.1), to the conservation equation

$$\frac{\partial(\rho u Z)}{\partial x} + \frac{\partial(\rho v Z)}{\partial y} = \frac{\partial}{\partial y}\left(T^{\sigma}\frac{\partial Z}{\partial y}\right) + \alpha n \dot{m}_d, \tag{6.1}$$

for the gas-phase mixture-fraction variable

$$Z = \frac{S Y_{\scriptscriptstyle F} - \hat{Y}_{\scriptscriptstyle O} + 1}{S+1} \tag{6.2}$$

commonly employed in combustion. Equation (6.1) clearly demonstrates that, for spray combustion, this mixture-fraction variable fundamentally is not a conserved scalar, in the sense that it has a source associated with droplet vaporization. A closer look reveals that the source term $\dot{m}_d$ is non-zero only in regions where fuel vapor is generated, which suggests that Z behaves as a conserved scalar on both sides of the vaporization layer. The source term $\dot{m}_d$ becomes localized in space in the sheath-vaporization limit that is approached sufficiently far downstream. Near the ignition kernel, however, the thickness of the vaporization layer is comparable to the mixing-layer thickness, with the consequence that typically there is no localization of $\dot{m}_d$ in mixture-fraction space (Martínez-Ruiz *et al.* 2013). Gas-phase mixture fractions analogous to (6.2) have been used widely in turbulent spray flames for analyses of DNS results (Reveillon & Vervisch 2005; Luo *et al.* 2011) and for flamelet combustion modeling with finite-rate chemistry (Baba & Kurose 2008; Franzelli *et al.* 2013).

To make matters worse, the mixture fraction Z, as defined in Eqs. (6.1) or (6.2), is not always a single-valued function of the transverse coordinate in the mixing layer of the spray. This is clearly shown in Figure 5(a) for the flow field near the ignition kernel. It is observed that Z varies from near-stoichiometric conditions in the spray stream ($y \to -\infty$) because of the absence of fuel vapor there, reaches a maximum within the vaporization zone, and then decays to $Z = 0$ in the hot-air stream ($y \to +\infty$). In this case since none of the fuel is vaporized in the feed stream of the spray, $Z = Z_{st} = 1/(1+S)$ there according to (6.2). As a result, the dimensionless scalar dissipation rate χ nondimensionalized with $\rho_{\scriptscriptstyle A}/t_v$, which is defined here as

$$\chi = T^{\sigma}\left(\frac{\partial Z}{\partial y}\right)^2 \tag{6.3}$$

(to leading order in 1/Pe for strained mixing layers), reaches zero within the vaporization

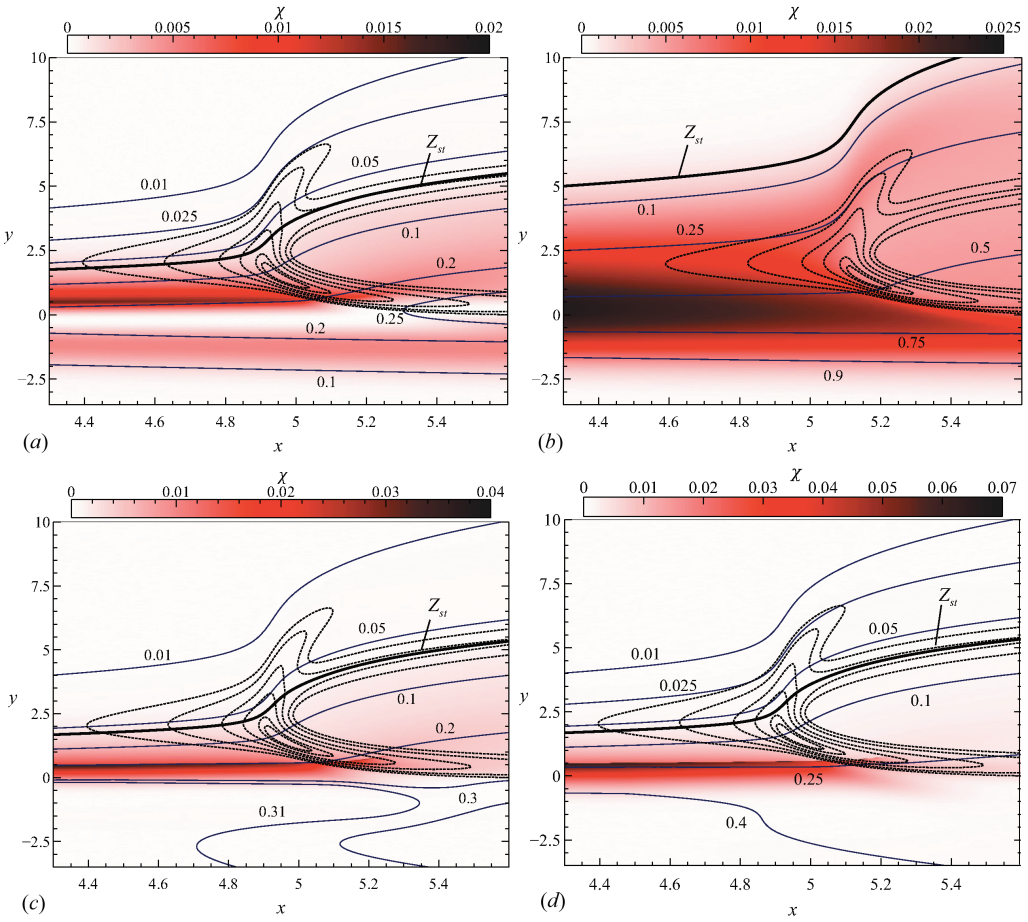

FIGURE 5. Contours of the mixture fraction Z (solid lines), computed from (a) Eq. (6.2), (b) Eq. (6.7), (c) Eq. (6.8) and (d) Eq. (6.10), overlaid on reaction rate isocontours (dashed lines) and filled contours of the scalar dissipation rate χ (color online), for the same conditions as in Figure 3(a).

region $y \simeq 0$ as shown by the colored contours of Figure 5(a). It is also observed in Figure 5(a) that ignition by thermal runaway occurs in regions of low scalar dissipation rate immediately above the vaporization region where fuel vapor is available in a high-temperature region. An asymptotic expansion of χ can be obtained in this region as $\chi_\infty = A_Z^2 \exp\{-2[\mathrm{erfc}^{-1}(2Z/A_Z)]^2\}/(2\pi x')$, where $x' = x - x_Z$ is the streamwise coordinate corrected with a virtual origin x_Z, and A_Z is an integration constant. By way of contrast, in laminar gaseous diffusion flames the scalar dissipation rate is a bell-shaped curve similar to χ_∞ up to factors and time translations, with $\chi = 0$ only at the two free streams $Z = 0$ and $Z = 1$, quite different from that shown in Figure 5(a) (Peters 2000).

6.2. *Gas-phase flamelet equations for the igniting mixing layer*

Use of flamelet equations for gaseous fuels generally involves modeling of $\chi(Z)$. For sprays, models for the distributions $n(Z)$, $\dot{m}_d(Z)$, $\dot{q}_d(Z)$, and $T_d(Z)$ also are needed. Plots of these distributions in $Z-$space are given in Martínez-Ruiz *et al.* (2013) for the present spray problem. For non-volatile sprays, combustion may occur near or within the

spray cloud, and associated flamelet calculations would necessarily involve modeling of these terms. If the gas-phase mixture fraction (6.1)-(6.2) is used, ignition in unstrained mixing layers may be addressed in Z space by expressing Eqs. (4.3)-(4.5) as

$$\rho\frac{\partial Y_{F}}{\partial t}+\alpha n\dot{m}_{d}\left[\frac{\partial Y_{F}}{\partial Z}(1-Z)-(1-Y_{F})\right]=\chi\frac{\partial^{2}Y_{F}}{\partial Z^{2}}-\Delta\Omega, \tag{6.4}$$

$$\rho\frac{\partial \hat{Y}_{O}}{\partial t}+\alpha n\dot{m}_{d}\left[\frac{\partial \hat{Y}_{O}}{\partial Z}(1-Z)+\hat{Y}_{O}\right]=\chi\frac{\partial^{2}\hat{Y}_{O}}{\partial Z^{2}}-S\Delta\Omega, \tag{6.5}$$

$$\rho\frac{\partial T}{\partial t}+\alpha n\left\{\dot{q}_{d}+\dot{m}_{d}\left[\ell_{v}+T-T_{d}+(1-Z)\frac{\partial T}{\partial Z}\right]\right\}=\chi\frac{\partial^{2}T}{\partial Z^{2}}+q\Delta\Omega, \tag{6.6}$$

in which unity Lewis numbers have been assumed, and in which the change of variables $x\rightarrow t$ has been performed. The presence of the additional terms within curly brackets in (6.4)–(6.6) is due to the vaporization of the spray. The form of (6.4)-(6.6) is independent of the flow configuration to the extent that Z-field curvature effects are negligible. These particular equations represent the flamelet equations for the combustion of equidiffusive monodisperse sprays with finite-rate chemistry.

6.3. *Other mixture fractions in spray combustion*

Often in computational approaches, instead of using Eqs. (6.1) or (6.2), the mixture fraction is obtained by solving an approximate differential equation free from source terms,

$$\frac{\partial(\rho uZ)}{\partial x}+\frac{\partial(\rho vZ)}{\partial y}=\frac{\partial}{\partial y}\left(T^{\sigma}\frac{\partial Z}{\partial y}\right), \tag{6.7}$$

along with other conservation equations (Pitsch & Peters 1998; Knudsen & Pitsch 2010; Shashank 2012), and subject to $Z=0$ and $Z=1$ in the oxidizer and fuel streams, respectively. The non-conservative version of (6.7), which in gaseous combustion is source-free, leads to the cancellation of the convective terms in the gaseous flamelet equations (Peters 2000), and also in Eqs. (6.4)-(6.6). The results of the integration of Eq. (6.7) are shown in the isocontours of Figure 5(b). Specifically, Eq. (6.7) appears to yield monotonic values for the mixture fraction and single-valued mapping between other variables and Z. However, this definition does not eliminate the need of modeling the spray-source terms in the flamelet equations. The three-dimensional time-dependent version of Eq. (6.7) is often used to solve for the mixture fraction in turbulent fields, tabulating and linking it to a flamelet subproblem written in terms of Z as an independent variable (Peters 2000). Nonetheless, Eq. (6.7) or its three-dimensional time-dependent version cannot be derived from linear combinations of the conservation equations in spray combustion due to the presence of the spray-source terms. In addition, the resulting location of the stoichiometric mixture fraction $Z_{st}=1/(1+S)$ in physical space is not related in any way to the flame position. Such a source-free conservation equation is, however, more attractive computationally than (6.1) because the latter requires closure modeling for the spray-vaporization term in both the filtered equation and the associated conservation equation for the subgrid variance.

Other definitions of the mixture fraction may involve the additional consideration of the liquid-fuel mass fraction, $Y_{F,L}=\alpha na^{3}/\rho$, for instance

$$Z=\frac{S(Y_{F}+Y_{F,L})-\hat{Y}_{O}+1}{1+S}, \tag{6.8}$$

which gives the transport equation

$$\frac{\partial(\rho u Z)}{\partial x}+\frac{\partial(\rho v Z)}{\partial y}=\frac{\partial}{\partial y}\left(T^{\sigma}\frac{\partial Z}{\partial y}\right)+\frac{\alpha n\dot{m}}{(1+S)}$$
$$+\frac{S}{1+S}\left\{\frac{\partial[\rho(u-u_d)Y_{F,L}]}{\partial x}+\frac{\partial[\rho(v-v_d)Y_{F,L}]}{\partial y}-\frac{\partial}{\partial y}\left(T^{\sigma}\frac{\partial Y_{F,L}}{\partial y}\right)\right\}, \tag{6.9}$$

where use has been made of Eqs. (4.1), (4.4), (4.3) and (4.6). Conversely, if the mass fractions of fuel and oxygen based on the total mixture mass (e.g. including the liquid-phase mass) are utilized in (6.8) to define the mixture fraction as

$$Z=\frac{SY_{F}-\hat{Y}_{O}+1}{1+S}+Y_{F,L}, \tag{6.10}$$

the transport equation for Z becomes

$$\frac{\partial}{\partial x}(\rho u Z)+\frac{\partial}{\partial y}(\rho v Z)=\frac{\partial}{\partial y}\left(T^{\sigma}\frac{\partial Z}{\partial y}\right)$$
$$+\frac{\partial[\rho(u-u_d)Y_{F,L}]}{\partial x}+\frac{\partial[\rho(v-v_d)Y_{F,L}]}{\partial y}-\frac{\partial}{\partial y}\left(T^{\sigma}\frac{\partial Y_{F,L}}{\partial y}\right). \tag{6.11}$$

The numerical evaluation of Eq. (6.8) shown in Figure 5(c) reveals that this definition of Z offers little advantage in this problem. On the contrary, Figure 5(d) shows that (6.10) may be of some interest for modeling since it appears to be mostly monotonic in the region of interest, although it departs strongly from monotonicity in the region upstream (not shown). Consideration of the fuel in liquid phase, however, requires modeling additional terms that are proportional to the liquid-gas slip velocity. These terms can be important in order-unity Stokes-number flows and appear explicitly in the equation of Z because the liquid mass fraction is not transported by the gas velocity. Furthermore, penalty terms of liquid-gas cross-diffusion arise in Eqns. (6.9) and (6.11) since droplets of realistic sizes cannot be transported by molecular diffusion as gaseous fuel molecules are transported. In this regard, singularities may arise in the derivatives of Z since the liquid mass fraction is transported hyperbolically by the spray velocity. Lastly, in addition to the unclosed terms $\chi(Z)$, $\dot{m}_d(Z)$, $T_d(Z)$, and $n(Z)$, the corresponding flamelet equations obtained by using (6.9) or (6.11) would contain the unknown distribution $Y_{F,L}(Z)$.

In the limit of infinitely-fast chemistry, which applies, for instance, to the description of nonpremixed sprays in coflow mixing layers far downstream from the ignition point, a mixture-fraction formulation derived from first principles, which requires the computation of the solution to an additional excess-enthalpy equation, has been proposed and utilized in recent work (Arrieta-Sanagustín *et al.* 2013; Martínez-Ruiz *et al.* 2013). This formulation could be easily extended to tackle the diffusive combustion of turbulent fuel sprays.

7. Conclusions

In this study, laminar spray-combustion models were formulated to characterize fundamental ignition kernels in both non-premixed and partially premixed spray systems. Considerations were also are given to characterize different ignition regimes in turbulent mixing layers. Finally, results were calculated for the distributions of mixture fraction and scalar dissipation rate that reveal complexities that serve to identify challenging differences between spray-flamelet and gaseous-flamelet problems.

Acknowledgments

This work was funded by the Spanish MCINN Project # CSD2010-00010 and by the AFOSR Grant # FA9550-12-1-0138. Javier Urzay was supported by the 2011-2012 Postdoctoral Fellowship for Excellence in Research, Ibercaja Foundation (Zaragoza, Spain). This investigation was completed during a 2-month stay of Daniel Martínez-Ruiz at CTR.

REFERENCES

Arrieta-Sanagustín, J., Sánchez, A. L., Liñán, A. & Williams, F. A. 2013 Coupling-function formulation for monodisperse spray diffusion flames with infinitely fast chemistry. *Fuel Process. Technol.* **107**, 81–92.

Baba, Y. & Kurose, R. 2008 Analysis and flamelet modeling for spray combustion. *J. Fluid Mech.* **612**, 45–79.

Bilger, R. W. 2011 A mixture fraction framework for the theory and modeling of droplets and sprays. *Combust. Flame* **158**, 191–202.

Franzelli, B., Fiorina B. & Darabiha, N. 2013 A tabulated chemistry method for spray combustion. *Proc. Comb. Inst.* **34**, 1659–1666.

Knudsen, E. & Pitsch, H. 2010 Large eddy simulation of a spray combustor using a multi-regime flamelet approach. In *Annual Research Briefs,* pp. 337–350. Center for Turbulence Research.

Li, S. C. 1997 Spray stagnation flames. *Prog. Ener. and Comb. Sci.* **23**, 303–347.

Liñán, A. 1985 Theory of droplet vaporization and combustion, in *Modélisation des Phénomènes de Combustion* R. Borghi, P. Clavin, A. Liñán, P. Pelcé, and G. I. Sivashinsky, eds., CEA-EDF INRIA 59. Editions Eyrolles, pp. 73–103.

Liñán, A. & Crespo, A. 1976 An asymptotic analysis of unsteady diffusion flames for large activation energies. *Combust. Sci. Technol.* **14**, 95–117.

Longmire, E. & Eaton, J. K. 1992 Structure of a particle-laden round jet. *J. Fluid. Mech.* **236**, 217–257.

Luo, K., Pitsch, H., Pai, M. G. & Desjardins, O. 2011 Direct numerical simulations and analysis of the three-dimensional n-heptane spray flames in a model swirl combustor. *Proc. Comb. Inst.* **33**, 2143–2152.

Mastorakos, E. 2009 Ignition of turbulent non-premixed flames. *Prog. Ener. Comb. Sci.* **35**, 57–97.

Peters, N. 2000 *Turbulent Combustion*, Cambridge University Press.

Pitsch, H. & Peters, N. 1998 A consistent flamelet formulation for non-premixed combustion considering differential diffusion effects. *Comb. Flame* **114**, 26–40.

Reveillon, J. & Vervisch, L. 2005 Analysis of weakly turbulent dilute-spray flames and spray combustion regimes. *J. Fluid Mech.* **537**, 317–347.

Shashank 2011 *High-fidelity simulations of reactive liquid-fuel jets*, Ph.D. Thesis, Stanford University.

Martínez-Ruiz, D., Urzay, J., Sánchez, A. L., Liñán, A. & Williams, F. A. 2013 Dynamics of thermal ignition of spray flames in mixing layers. *J. Fluid Mech.* **734**, 387–423.

Wang, Y. & Rutland, C. J. 2007 Direct numerical simulation of ignition in turbulent n-heptane liquid-fuel spray jets. *Combust. Flame* **149**, 353–365.

Williams, F. A. 1985 *Combustion Theory*, Second ed., Benjamin Cummings, Menlo Park, CA, pp. 446–484.